

# Static properties of small Josephson tunnel junctions in an oblique magnetic field

R. Monaco\*

*Istituto di Cibernetica del CNR, 80078, Pozzuoli, Italy and Dipartimento di Fisica, Unità INFM, Università di Salerno, 84081 Baronissi, Italy*

M. Aaroe and J. Mygind

*DTU Physics, B309, Technical University of Denmark, DK-2800 Lyngby, Denmark*

V. P. Koshelets

*Kotel'nikov Institute of Radio Engineering and Electronics, Russian Academy of Science, Mokhovaya 11, B7, 125009, Moscow, Russia*

(Received 15 January 2009; revised manuscript received 11 March 2009; published 22 April 2009)

We have carried out a detailed experimental investigation of the static properties of planar Josephson tunnel junctions in presence of a uniform external magnetic field applied in an arbitrary orientation with respect to the barrier plane. We considered annular junctions, as well as rectangular junctions (having both overlap and cross-type geometries) with different barrier aspect ratios. It is shown how most of the experimental findings in an oblique field can be reproduced invoking the superposition principle to combine the classical behavior of electrically small junctions in an in-plane field together with the small junction behavior in a transverse field that we recently published [R. Monaco *et al.*, *J. Appl. Phys.* **104**, 023906 (2008)]. We show that the presence of a transverse field may have important consequences, which could be either voluntarily exploited in applications or present an unwanted perturbation.

DOI: 10.1103/PhysRevB.79.144521

PACS number(s): 74.50.+r

## I. INTRODUCTION

One of the earliest experiments involving Josephson junctions and magnetic fields has been the measurement of the magnetic diffraction pattern,<sup>1</sup> i.e., the dependence of the junction critical current  $I_c$  on the amplitude of an externally applied magnetic field  $\mathbf{H}_a$ . Traditionally, since the discovery of the Josephson effect in 1962, the magnetic diffraction pattern  $I_c(H_a)$  of planar Josephson tunnel junctions (JTJs) has been recorded with the magnetic induction field applied in the junction plane to avoid the huge computational complications of taking demagnetization effects into account, when a transverse magnetic component is present. A number of important results have been derived from experiments under these assumptions—a prominent example being the determination of the London penetration depth<sup>2</sup>  $\lambda_L$  from which one derives the Josephson penetration depth<sup>3</sup>  $\lambda_J$  which sets the JTJ electric length scale. Nowadays, every textbook on the Josephson effect deserves at least one chapter to the magnetic diffraction phenomena. The simplest case is that sketched in Fig. 1 of a rectangular JTJ placed in a uniform and constant external magnetic field parallel to one of the barrier edges. Let us choose the coordinate system such that the tunnel barrier lies in the  $z=0$  plane and let  $2L$  and  $2W$  be the junction dimensions along the  $x$  and  $y$  directions, respectively. Finally, let us assume that the JTJ is electrically small, meaning that its dimensions are both smaller than the Josephson penetration depth ( $2L, 2W < \lambda_J$ ) (absence of self-fields) and that its Josephson current density  $J_J$  is constant over the barrier area.

If the externally applied field  $\mathbf{H}_a$  is along the  $x$  direction  $\mathbf{H}_a = H_x \hat{\mathbf{x}}$  then the magnetic field  $\mathbf{H}$  inside the junction is constant and equal to the external value, i.e.,  $\mathbf{H} \equiv (H_x, 0, 0)$ . By integrating the Josephson equation<sup>3</sup> relating the Josephson phase  $\phi$  to the magnetic induction field in the barrier  $\mathbf{H}$ ,

$$\nabla \phi(x, y) = \frac{2\pi d_e \mu_0}{\Phi_0} \mathbf{H}(x, y) \times \hat{\mathbf{z}}, \quad (1)$$

in which  $d_e$  is the junction magnetic thickness,  $\mu_0$  is the vacuum permeability, and  $\Phi_0 = h/2e$  is the magnetic-flux quantum, we readily obtain the spatial dependence of the Josephson phase,

$$\phi = \kappa H_x y, \quad (2)$$

with  $\kappa = 2\pi d_e \mu_0 / \Phi_0$ . Equation (2) leads to the well-known Fraunhofer-type magnetic diffraction pattern,<sup>3</sup>

$$I_c(H_x) = I_0 \left| \frac{\sin \pi H_x / H_c}{\pi H_x / H_c} \right|, \quad (3)$$

where  $I_0 = 4J_J WL$  is the zero-field junction critical current and  $H_c = \Phi_0 / 2\mu_0 d_e L$  is the so-called (*first*) critical field, i.e., the smallest field value for which the Josephson current vanishes. Barone and Paternò<sup>4</sup> generalized Eq. (3) to the case of an arbitrary orientation of the external magnetic field in the junction plane  $\mathbf{H}_a = H_x \hat{\mathbf{x}} + H_y \hat{\mathbf{y}}$ . In such a case, still  $\mathbf{H} = \mathbf{H}_a$  and the resulting magnetic diffraction pattern will be

$$I_c(H_x, H_y) = I_0 \left| \frac{\sin \pi H_x / H_{cx}}{\pi H_x / H_{cx}} \times \frac{\sin \pi H_y / H_{cy}}{\pi H_y / H_{cy}} \right|, \quad (4)$$

with  $H_{cx} = \Phi_0 / 2\mu_0 d_e L$  and  $H_{cy} = \Phi_0 / 2\mu_0 d_e W$ . Unfortunately, the last equation cannot be easily generalized to the case of an arbitrary applied field orientation  $\mathbf{H}_a = H_x \hat{\mathbf{x}} + H_y \hat{\mathbf{y}} + H_z \hat{\mathbf{z}}$ , simply because when  $H_z \neq 0$  then  $\mathbf{H} \neq \mathbf{H}_a$ . The effect of a transverse magnetic field has been first considered in 1975 by Hebard and Fulton<sup>5</sup> in order to provide a correct interpretation to some experimental data published in the same year.<sup>6</sup> They observed that a transverse applied field  $\mathbf{H}_a = H_z \hat{\mathbf{z}}$  induces Meissner surface demagnetizing currents  $\mathbf{j}_s$  feeding the

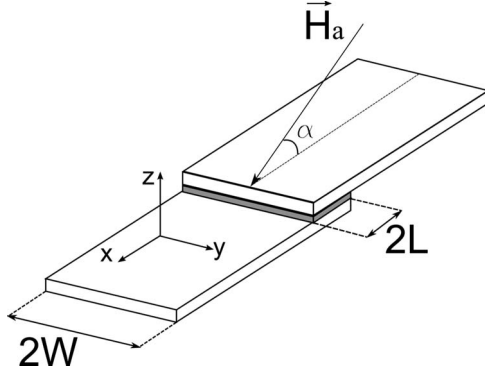


FIG. 1. Sketch of a rectangular planar Josephson tunnel junction. The tunnel barrier lies in the  $z=0$  plan. An oblique field  $\mathbf{H}_a$  is applied in the  $x$ - $z$  plane and forms an angle  $\alpha$  with respect to the  $x$  direction.

interior of the junction and so generating a magnetic field  $\mathbf{H}$  in the barrier plane such that  $\mathbf{j}_s = \hat{\mathbf{z}} \times \mathbf{H}$ . The problem of finding the  $\mathbf{j}_s$  distribution in a single superconducting film subjected to a transverse magnetic field has been analytically solved for different film geometries.<sup>7,8</sup> However, a planar JTJ is made by two overlapping superconducting films separated by a thin dielectric layer and the Meissner current distributions on the interior surfaces (top surface of the bottom film and bottom surface of the top film) require numerical approaches even for the more tractable electrode configurations. Recently,<sup>9</sup> the magnetic field distribution  $\mathbf{H}^\perp$  in the barrier of small planar JTJs has been numerically obtained in the case when an external magnetic field is applied perpendicular to the barrier plane  $\mathbf{H}_a = (0, 0, H_z)$ . The simulations allowed for heuristic analytical approximations for the Josephson static phase profile  $\phi^\perp$  from which the dependence of the maximum Josephson current  $I_c(H_z)$  on the applied field amplitude was calculated for the most common electrode geometrical configurations (overlap, cross, and annular junctions). Unfortunately, the theoretical findings could not be tested against experimental results due to the insufficiency of data available in the literature.

One of the aims of this paper is to fill this vacancy. We have measured the transverse magnetic diffraction patterns of several planar JTJs with the most common geometrical configurations and compared the results with their expected counterparts. More generally, we have recorded the  $I_c(H_a)$  when the applied field is oblique, that is, has nonzero in-plane and transverse components. To avoid complications and without loss of generality, we have chosen the in-plane component to be along one of the electrode axis—more specifically—along the  $x$  direction,

$$\mathbf{H}_a = H_x \hat{\mathbf{x}} + H_z \hat{\mathbf{z}}, \quad (5)$$

so that, as shown in Fig. 1, the applied field forms an angle  $\alpha$  with respect to the  $x$ - $y$  plane, that is,

$$H_x = H_a \cos \alpha, \quad H_z = H_a \sin \alpha, \quad (6)$$

with  $H_a = \sqrt{H_x^2 + H_z^2}$ . We will demonstrate that the experimental oblique magnetic diffraction patterns can be nicely reproduced by properly extending the theoretical framework of

Ref. 9. This paper is constructed as follows. In Sec. II we will present the samples used for the measurements and describe the experimental setup. Section III will report on the experimental results obtained for those samples whose barrier has a rectangular shape (overlap-type junctions in Sec. III A and cross-type junctions in Sec. III B). Section III C will be devoted to the annular JTJs. Then, in Sec. IV we will discuss how to generalize the theoretical analysis of the effect of a transverse magnetic field to the case of an oblique field. Finally, the discussion and the interpretation of the measurements will be given in Sec. V, while the conclusions will be presented in Sec. VI.

## II. SAMPLES

High-quality Nb/Al-Al<sub>ox</sub>/Nb JTJs were fabricated on 0.35-mm-thick silicon substrates using the trilayer technique in which the junction is realized in the window opened in a SiO<sub>2</sub> insulator layer—details of the fabrication process can be found in Ref. 10. The so-called passive or *idle* region, i.e., the distance of the barrier borders to the electrode borders, was on the order of 1–2  $\mu\text{m}$  for all the junctions. The thickness of the SiO<sub>2</sub> insulator layer was 400 nm. The demagnetization currents strongly depend on the electrode thicknesses relative to the London penetration depth. For our samples the nominal thicknesses of the base, top, and wiring Nb layers were 200, 100, and 500 nm, respectively. Considering that the London penetration depth for Nb film is  $\lambda_L \approx 90$  nm,<sup>2</sup> we see that our samples satisfy the thick-film approximation. For all samples, the high quality has been inferred by a measure of the I-V characteristic at  $T=4.2$  K. In fact, the subgap current  $I_{sg}$  at 2 mV was small compared to the current rise  $\Delta I_g$  in the quasiparticle current at the gap voltage  $V_g$ , typically  $\Delta I_g > 20I_{sg}$ ; the gap voltage was as large as  $V_g = 2.8$  mV. The geometrical and electrical (at 4.2 K) parameters of the seven samples quoted in this paper are listed in Table I. For the rectangular junctions #A-F, beside their dimensions  $2L$  and  $2W$  along the  $x$  and  $y$  directions, respectively, we also report the junction aspect ratio  $\beta = L/W$ . (As shown in Ref. 9, this geometrical parameter turns out to be crucial for the magnetic field line distribution in the barrier of a JTJ subjected to a transverse magnetic field.) All the samples belonged to the same fabrication batch (except sample #C). Let us observe that for the overlap-type junctions #A and #B, the zero-field critical current  $I_0$  was as large as the theoretical value  $0.7\Delta I_g$  predicted for strong-coupling Nb-Nb JTJs, indicating the absence of self-field effects. The critical current density has been calculated as<sup>11</sup>  $J_c = 0.7\Delta I_g/A$  in which  $\Delta I_g$  is the measured quasiparticle current step at the gap voltage and  $A$  is the junction nominal area [ $A = 2L \times 2W$  for rectangular junctions and  $A = \pi(r_o^2 - r_i^2)$  for the annular junction]. The Josephson critical current density was  $J_c = 3.9$  kA/cm<sup>2</sup> for all samples, except for sample #C having  $J_c = 80$  A/cm<sup>2</sup>. The values of the barrier magnetic thickness  $d_e = 2\lambda_L \approx 180$  nm has been used to calculate the Josephson penetration depth  $\lambda_J = \sqrt{\phi_0/2\pi\mu_0 d_e J_c}$ . (In the thin-film limit,  $\lambda_J$  can be better determined by using the expression for  $d_e$  found by Weinhacht.<sup>12</sup>) Accordingly, all samples had  $\lambda_J \approx 6$   $\mu\text{m}$ , except sample #C which had  $\lambda_J$

TABLE I. Relevant electrical (at  $T=4.2$  K) and geometrical parameters of the rectangular and annular Nb/Al<sub>ox</sub>/Nb Josephson tunnel junctions quoted in this paper. The Josephson critical current density was  $J_c=3.9$  kA/cm<sup>2</sup> (corresponding to  $\lambda_J\simeq 6$   $\mu\text{m}$ ) for all samples, except for sample #C having  $J_c=80$  A/cm<sup>2</sup> ( $\lambda_J\simeq 42$   $\mu\text{m}$ ). The experimental results obtained for these samples will be presented in Sec. III as follows: overlap-type junctions in Sec. III A, cross-type junctions in Sec. III B, and annular junctions in Sec. III C.

$JJ$	Geometry	$2L \times 2W$ ( $\mu\text{m}^2$ )	$\beta L/W$	$I_0$ (mA)	$\Delta I_g$ (mA)	$\Delta_R^{\parallel}$ ( $\mu\text{T}$ )	$\Delta_R^{\perp}$ ( $\mu\text{T}$ )	$\eta_R$	$\Delta_R^{\perp}/\Delta_R^{\parallel}$	$\alpha_M$
A	overlap	$10 \times 10$	1	3.9	5.6	1290	1100	0.85		$140^\circ$
B	overlap	$5 \times 20$	0.25	3.9	5.6	550	190	0.35		$160^\circ$
C	overlap	$4 \times 500$	0.008	1.0	2.3	12	0.88	0.073		$176^\circ$
D	overlap	$20 \times 5$	4	3.6	5.6	2940	5400	1.84		$107^\circ$
E	Cross	$10 \times 10$	1	3.8	5.8	1080	810	0.75		
F	Cross	$20 \times 5$	4	3.0	5.4	420	2240	5.3		
$JJ$	Geometry	$r_i$ ( $\mu\text{m}$ )	$r_o$ ( $\mu\text{m}$ )	$I_0$ (mA)	$\Delta I_g$ (mA)	$\Delta_A^{\parallel}$ ( $\mu\text{T}$ )	$\Delta_A^{\perp}$ ( $\mu\text{T}$ )	$\eta_A$	$\Delta_A^{\perp}/\Delta_A^{\parallel}$	$\alpha_M$
G	annular	5	8	4.3	6.4	490	310	0.63		$145^\circ$

$\simeq 42$   $\mu\text{m}$ . In other words, as far as the electrical length concerns, all samples can be classified as intermediate length junctions ( $2L, 2W \simeq \lambda_J$ ), except sample #C, that is, a long ( $2L \gg \lambda_J$ ) unidimensional ( $2W \ll \lambda_J$ ) overlap-type JTJ.

We now come to the definition of the parameters  $\Delta_R^{\parallel}$ ,  $\Delta_R^{\perp}$ , and their ratio  $\eta_R$  whose experimental values are reported in Table I for the rectangular junctions ( $\Delta_A^{\parallel}$ ,  $\Delta_A^{\perp}$ , and  $\eta_A$  for the annular junction). As already mentioned in Sec. I, it is well known that the magnetic diffraction pattern of an electrically small rectangular JTJ in the presence of an in-plane field perpendicular to one of the barrier edge follows the Fraunhofer pattern in Eq. (3) characterized by a periodic amplitude modulation. As depicted in Fig. 2, the value  $H_c$  of the applied field where first the critical current vanishes is called the (first) critical field. For those samples whose  $I_c(H_a)$  is still amplitude modulated but follows a different pattern (for example, annular, circular, and rhombic junctions), the critical field  $H_c$  can still be defined as that value of external field  $H_a$  where first the critical current nulls  $I_c(H_c)=0$ . Further, for

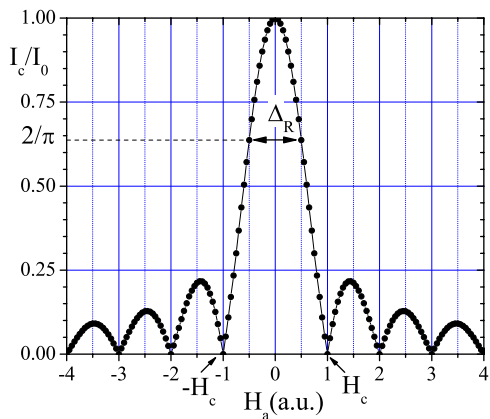


FIG. 2. (Color online) Definition of the parameter  $\Delta_R$  as the width of the magnetic field range in which  $I_c(H_a)\geq(2/\pi)I_0$ . By definition, for a Fraunhofer-type magnetic diffraction pattern,  $\Delta_R$  coincides with the junction (first) critical field  $H_c$ .

those samples whose  $I_c(H_a)$  shows modulation lobes but never vanishes (for example, the small junction with nonuniform tunneling current and long JTJs), the critical field can still be obtained extrapolating to zero the first modulation lobe. However, in those cases in which the critical current  $I_c$  is a monotonically decreasing function of the applied field  $H_a$ , the concept of critical field  $H_c$  loses its meaning and a new feature has to be introduced to characterize the behavior of  $I_c(H_a)$  for small fields. A theoretical example is offered by a Gaussian-shaped junction subjected to an in-plane magnetic field that is characterized by a Gaussian magnetic diffraction pattern.<sup>13</sup> A practical example is given by a square cross junction in a transverse field, whose  $I_c(H_a)$  decreases with  $H_a$  with no measurable modulation.<sup>14</sup> The experimental magnetic diffraction patterns that will be reported in Sec. III span all kinds of behaviors from Fraunhofer-type to  $1/H_a^\nu$  type (with  $\nu>0$ ). Therefore, as the new and universal figure of merit to characterize the response of the critical current to the externally applied field amplitude, we have chosen the width of the magnetic field range  $\Delta_R$  in which  $I_c(H_a)\geq(2/\pi)I_0\simeq 0.64I_0$  (see Fig. 2). Considering that, when Eq. (3) holds,  $I_c(H_c/2)=(2/\pi)I_0$ , the value of the prefactor stems from the requirement that the new merit figure  $\Delta_R$  numerically equals the critical field  $H_c$  whenever the measured magnetic pattern follows a Fraunhofer dependence, i.e.,  $\Delta_R=H_c$ . In all other cases, generally speaking  $\Delta_R\neq H_c$ . In our notation,  $\Delta_R^{\parallel}$  and  $\Delta_R^{\perp}$  are the merit figures of, respectively, an in-plane ( $\alpha=0$ ) and transverse ( $\alpha=90^\circ$ ) magnetic diffraction patterns. With a similar reasoning, we define the parameter  $\Delta_A$  for annular junctions as the width of the magnetic field range  $\Delta_R$  in which  $I_c(H_a)\geq\mu I_0$ , with  $\mu\simeq 0.67$ . The slightly different prefactor stems from the fact that the in-plane diffraction pattern of a small annular junction (with no trapped fluxon) follows a Bessel-type dependence:<sup>15</sup>  $I_c(H_a)=I_0|J_0(\zeta_1 H_a/H_c)|$  in which  $J_0$  is the zero-order Bessel function and  $\zeta_1\approx 2.405$  is its first zero. Now  $H_c=\Phi_0/\mu_0 d_e C$ , where  $C$  is the ring mean circumference.

The measurement of  $\Delta$  requires an external field smaller than the one required for  $H_c$ ; henceforth, this new parameter

also turns out to be a very useful quantity whenever the junction critical field cannot be experimentally determined since it exceeds the irreversible field, i.e., when the Abrikosov vortices first enter into the superconducting films and become pinned in the junction.<sup>16</sup> For our samples, the transverse irreversible field was about 5 mT (50 G).

The ratios  $\eta_R = \Delta_R^\perp / \Delta_R^\parallel$  and  $\eta_A = \Delta_A^\perp / \Delta_A^\parallel$  provide a direct comparison between the  $I_c$  response to a transverse field relative to the in-plane field; specifically,  $\eta < 1$  means that the junction critical current modulates faster when the applied field is transverse. In a recent paper,<sup>17</sup> we already provided an experimental proof that a transverse magnetic field can be much more capable than an in-plane one to modulate the critical current  $I_c$  of a planar JTJ with proper barrier and electrodes geometry requirements. This property was first obtained and exploited in the context of a detailed investigation of the phase symmetry breaking during fast normal-to-superconducting phase transitions of long annular JTJs.<sup>18</sup>

Our setup consisted of a cryoprobe inserted vertically in a commercial LHe dewar. The cryoprobe was magnetically shielded by means of two concentric magnetic shields: the inner one made of Pb and the outer one of cryoperm. Inside the vacuum tight can of the cryoprobe, a nonmagnetic insert holds a chip mount with spring contacts to a Si chip with planar JTJs. With reference to the coordinate system in Fig. 1, the chip was positioned in the center of a long superconducting cylindrical solenoid whose axis was along the  $x$  direction (within less than  $1^\circ$  of accuracy) to provide an in-plane magnetic field. In order to provide a transverse magnetic field, a superconducting cylindrical coil was placed 5 mm far from the chip with its axis oriented along the  $z$  direction (within less than  $3^\circ$  of accuracy). Two independent low-noise dc current sources were used to feed the solenoid and the coil in order to expose our samples at magnetic fields having arbitrary magnitude and orientation (in the  $x$ - $z$  plane). The field-to-current ratio was  $3.9 \mu\text{T}/\text{mA}$  for the solenoid and  $4.4 \mu\text{T}/\text{mA}$  for the coil. These values have been numerically obtained from Comsol Multiphysics magnetostatic simulations in order to take into account the strong correction to the free-space solution due to the presence of the close fitting superconducting shield.<sup>19</sup>

### III. MEASUREMENTS

In this section we present the experimental oblique magnetic diffraction patterns relative to planar JTJs having the seven different electrode configurations listed in Table I. Section III A–III C will concern samples having, respectively, overlap, inline, and annular geometry. The theoretical interpretation of our data sets will be given in Sec. IV. The angle  $\alpha$  that the external oblique field forms with barrier plane could be experimentally spanned in the interval  $[-\pi, \pi]$ ; however, according to Eq. (6), an angle rotation of  $\pm\pi$  is equivalent to an inversion of the field direction, i.e., of the field amplitude  $H_a \rightarrow -H_a$ . For this reason, we will only present data for  $\alpha$  in the  $[0, \pi]$  interval with the amplitude  $H_a$  assuming both negative and positive values. Further, by denoting with  $I_c^+$  and  $I_c^-$  the positive and negative critical currents, respectively, we always had  $I_c^-(H_a) = I_c^+(-H_a)$ , as ex-

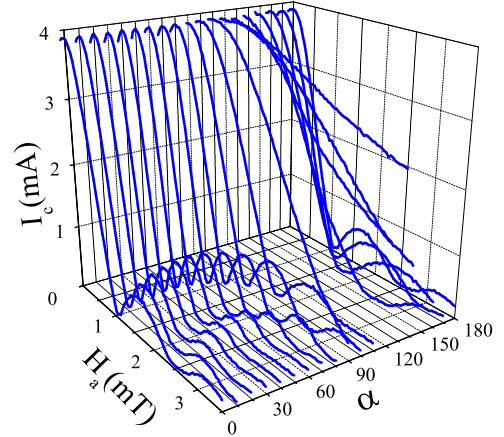


FIG. 3. (Color online) Tridimensional plot showing for the square overlap junction ( $\beta=1$ ) the recorded magnetic diffraction patterns  $I_c(H_a)$  for different values of the field orientation  $\alpha$  (with  $\Delta\alpha=10^\circ$ ).

pected, due to the absence of any measurable stray fields in our setup. For this reason, we will only present data for  $I_c^+$ , which we will simply call  $I_c$ . We stress that, in recording the  $I_c$  vs  $H_a$  curves, we took special care that the applied field never exceeded the reversible field, so it was not expected that the applied field penetrated the films. Furthermore, through measurements of the sample's I-V characteristic, it was verified that  $H_a$  was so small as not to affect the energy gap. Finally, the raw experimental data were postprocessed to take into account the difference in the solenoid and coil field-to-current factors.

#### A. Overlap-type junctions

We begin with an intermediate length square overlap-type JTJ, namely, sample #A in Table I ( $2L=2W \approx 1.6\lambda_J$ ). Figure 3 is a tridimensional plot of the magnetic diffraction patterns recorded for different  $\alpha$  values (with  $\Delta\alpha=10^\circ$ ). Since, for this sample,  $I_c(-H_a)=I_c(H_a)$ , we only show the data for  $H_a \geq 0$ . It is evident that  $I_c(H_a)$  smoothly, but drastically, changes with the field orientation  $\alpha$ . To be clearer, in Fig. 4 we report the magnetic patterns for four selected  $\alpha$  values. For  $\alpha=0$  the applied field is in the barrier plane ( $z=0$ ) and, as seen in Fig. 4(a),  $I_c(H_a)$  closely follows a Fraunhofer-type behavior, as expected. The small discrepancy between the experimental data (closed circles) and the Fraunhofer fit (solid line) can be ascribed to the fact that junction dimensions are slightly larger than the Josephson penetration depth. Increasing  $\alpha$ , in the beginning the junction critical field  $H_c$  (or equivalently the width of the pattern main lobe  $\Delta_R$  defined earlier) first slowly decreases until it reaches an absolute minimum when  $\alpha \approx 50^\circ$  [see Fig. 4(b)] and later on quickly increases until it reaches an absolute maximum when  $\alpha \approx 140^\circ$  [see Fig. 4(d)]. In Fig. 4(c) we also report the transverse ( $\alpha=90^\circ$ ) magnetic pattern to evidence how much it differs from a Fraunhofer dependence. It is worth stressing that whenever  $\alpha \neq 2m\pi$  (with integer  $m$ ), the magnetic diffraction pattern loses the modulation periodicity  $H_{cn} = nH_{c1}$  featuring the Fraunhofer behavior; more specifically,

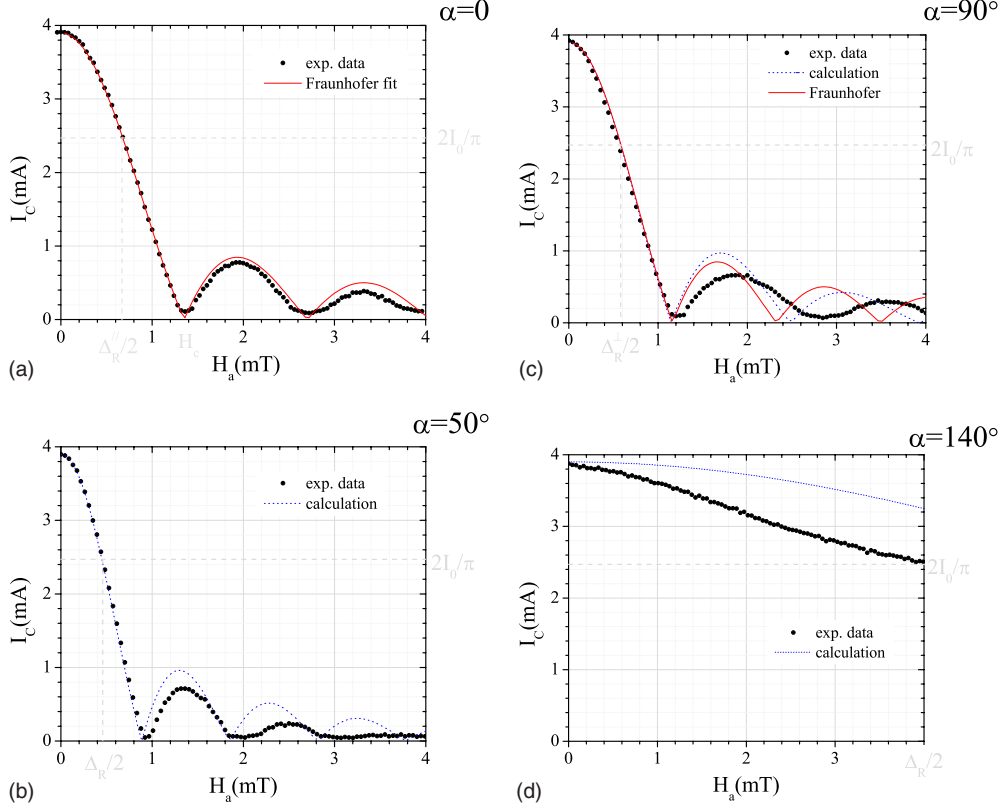


FIG. 4. (Color online) Magnetic diffraction patterns of the square overlap junction ( $\beta=1$ ) for different  $\alpha$  values: (a)  $\alpha=0$  (in-plane field), (b)  $\alpha=50^\circ$ , (c)  $\alpha=90^\circ$  (transverse field), and (d)  $\alpha=140^\circ$ . The experimental data are presented by closed circles. The solid lines, when present, are the best Fraunhofer fit, while the dotted lines are the results of the calculations described in Secs. IV. For  $\alpha=0$ , by construction, the calculations reproduce the Fraunhofer shape.

the distance between two adjacent minima increases as we move to larger fields, i.e.,  $H_{cn} > nH_{c1}$ . Each plot in Fig. 4 explicitly reports the corresponding position of the measured  $\Delta_R$ .

The  $\alpha$  dependence of  $\Delta_R$  (normalized to  $\Delta_R^{\parallel}$ ) for the sample #A is summarized in Fig. 5(a) (solid circles).  $\Delta_R(\alpha)$  is reported in Figs. 5(b)–5(d) for the samples #B, #C, and #D, overlap-type JTJs having aspect ratios, respectively,  $\beta=0.25$ , 0.08, and 4. The insets in Figs. 5(a)–5(d) sketch for each sample its electrode configuration and its orientation with respect to the Cartesian coordinates chosen in the Sec. I (see Fig. 1). We used a vertical log scale for those samples having  $\beta \leq 1$ . Each plot in Fig. 5 is characterized by an absolute maximum achieved when  $\alpha=\alpha_M$ . The  $\alpha_M$  values quoted in the last column of Table I were found to monotonically depend on the  $\eta_R$  ratios which, in turn, scale with the  $\beta$  ratios. In Sec. V we will discuss a simple theoretical approach aimed to find the  $\alpha$  dependence of  $\Delta_R$  and the relationship between  $\alpha_M$  and  $\eta_R$  as well.

We like to point out that the only measurements similar to those reported in Fig. 5 can be found in a pioneering paper dated 1975 by Rosenstein and Chen.<sup>6</sup> They measured the first and second junction critical fields in an oblique magnetic field for an overlap-type planar JTJ having  $\beta \approx 0.5$  (and formed by two 300-nm-thick Pb electrodes of unequal widths). They found that both  $H_{c1}$  and  $H_{c2}$  reach their maximum values when the field orientation is about  $8^\circ$  off the

in-plane direction ( $\alpha_M \approx 172^\circ$  in our notation). This value is consistent with our findings.

## B. Cross-type junctions

Figure 6 shows the transverse magnetic pattern of the square cross junction (sample #E in Table I) on a log-log plot. The inset displays the same data on linear scales. We observe that the critical current monotonically decreases as the external field is increased. The experimental data indicate that for large fields  $I_c \propto H_z^{-2}$ , in contrast with the simple inverse proportionality suggested by Miller *et al.*<sup>14</sup>

In Figs. 7(a) and 7(b), we report the oblique magnetic diffraction patterns of the two cross-type junctions quoted in Table I, respectively, JJ#E and JJ#F. For these samples, the in-plane patterns are skewed due to the self-field effects. The skewness is more pronounced for the asymmetric sample, having  $2L \approx 3\lambda_J$  and  $I_0 = I_c(H_a=0) = 3.6$  mA (of course  $I_0$  does not depend on  $\alpha$ ). As we move from an in-plane field (say  $\alpha=0$ ) to a transverse one (say  $\alpha=90^\circ$ ), the skewness gradually disappears and, keeping increasing  $\alpha$  toward  $180^\circ$ , the skewness changes its polarity; in other words,  $I_c(H_a, \pi/2+\alpha) = I_c(-H_a, \pi/2-\alpha)$ . For this reason, we only present the  $I_c(H_a, \alpha)$  plots for  $\alpha$  in the  $[\pi/2, \pi]$  range (with  $\Delta\alpha=15^\circ$ ). The two samples show a quite different  $\alpha$  dependence of the normalized pattern width  $\Delta_R/\Delta_R^{\parallel}$ , as shown in Fig. 8. While the former one is characterized by a weak

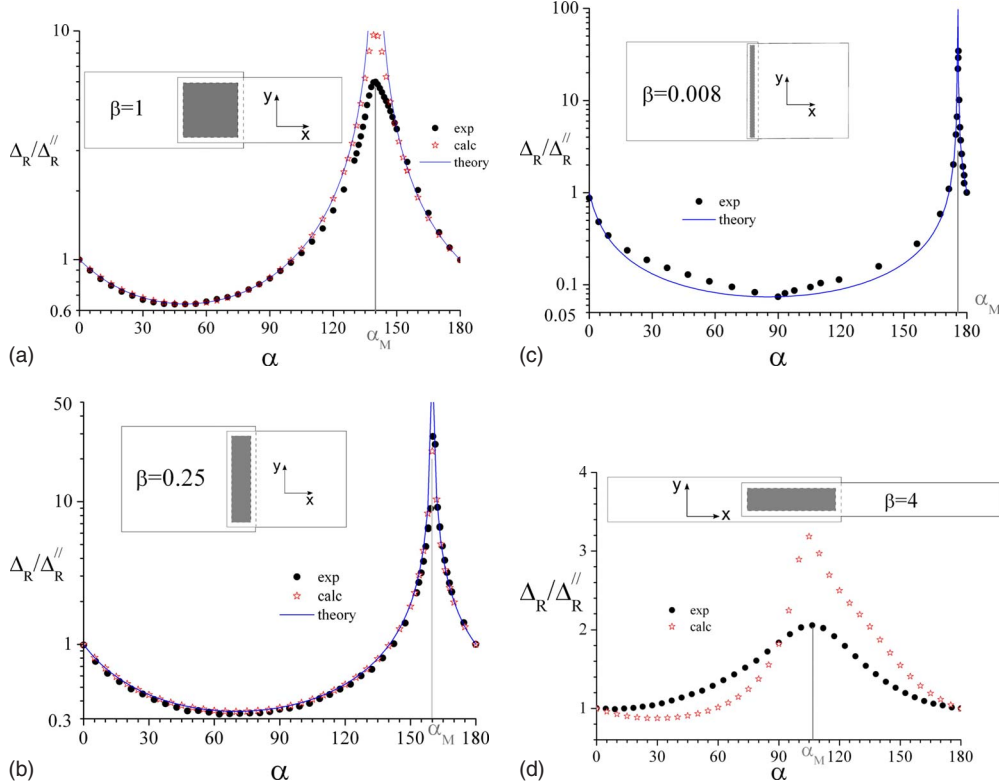


FIG. 5. (Color online) Magnetic field range  $\Delta_R$  vs  $\alpha$  (in degrees) for overlap junctions with different aspect ratios  $\beta$ : (a)  $\beta=1$ , (b)  $\beta=0.25$ , (c)  $\beta=0.08$ , and (d)  $\beta=4$ . The experimental data are presented by closed circles. The open stars result from the calculations described in Secs. IV, while the solid lines, when present, are the result of a simple theory developed in Sec. V. The insets sketch for each sample its electrode configuration and its orientation with respect to the chosen Cartesian coordinates.

dependence of  $\Delta_R(\alpha)$  with a minimum when the applied field is transverse, the latter one shows a substantial variation with a maximum when the applied field is close to be transverse, more specifically, when  $\alpha \approx 105^\circ$ .

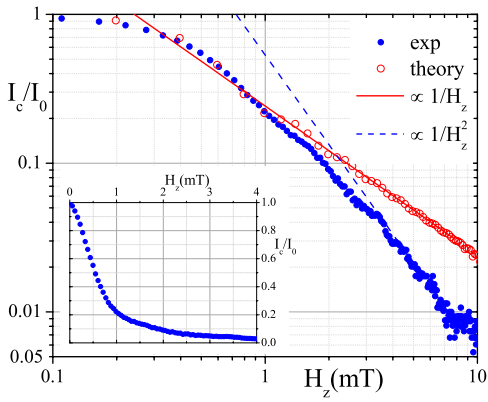


FIG. 6. (Color online) Log-log graph of the transverse magnetic pattern  $I_c(H_z)$  of the cross square junction. The closed squares are the experimental data, while the open circles are the result of computations based on Eq. (15). The dashed and solid lines are the large-field best fit of the experimental and computed data, respectively,  $\propto H_z^{-2}$  and  $\propto H_z^{-1}$ . The inset shows the experimental data on linear scales.

### C. Annular junctions

In two recent papers,<sup>9,17</sup> among other things, we have reported on the transverse magnetic diffraction patterns of ring-shaped Nb-based annular JTJs with radii ten times (or more) larger than the Josephson penetration depth. In this section, we present the results relative to a sample having the mean radius  $\bar{r} \approx \lambda_J$ , namely, JJ#G in Table I. Figure 9 compares in a combined plot the transverse and the in-plane recorded magnetic diffraction patterns: respectively, the open squares referred to top horizontal scale ( $H_z$ ) and the closed circles referred to the bottom horizontal scale ( $H_x$ ). The vertical logarithmic scale was needed to enhance the plot differences that would be otherwise barely observable using a vertical linear scale (a part of the quite different horizontal scales). On a first order of approximation, both patterns closely follow the zero-order Bessel function behavior; the solid line in Fig. 9 is the best data fit using Eq. (23) with the first critical field as a unique fitting parameter. Figure 9 indicates that for this particular sample, a transverse field modulates the junction critical current about 1.5 times faster than an in-plane field. In Ref. 17 we have shown that this gain increases with the ring diameter and can be even larger than 100.

As shown in Fig. 10, the annular range width  $\Delta_A$  drastically depends on the external field orientation  $\alpha$ . In fact, although its values for  $\alpha=0$  and  $90^\circ$  belong to the same order

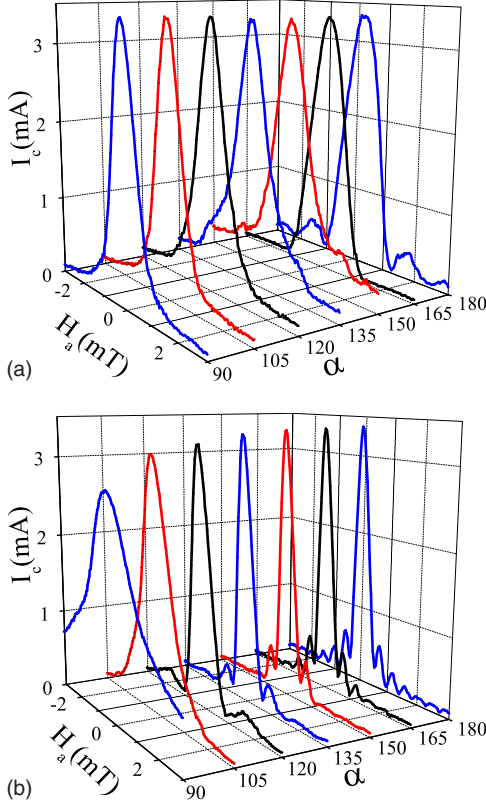


FIG. 7. (Color online) Tridimensional plots for the recorded oblique magnetic diffraction patterns  $I_c(H_a, \alpha)$  of two cross-type junctions: (a) square junction with  $\beta=1$  and (b) asymmetric junction with  $\beta=0.25$ . The angular separation is  $\Delta\alpha=15^\circ$ . [For these samples  $I_c(H_a, \pi/2+\alpha)=I_c(-H_a, \pi/2-\alpha)$ .]

of magnitude  $\Delta_A^\perp=0.63\Delta_A^\parallel$ , we see that  $\Delta_A(\alpha)$  is peaked at  $\alpha_M \approx 145^\circ$ , with  $\Delta_A(\alpha_M) \approx 100\Delta_A^\parallel \approx 160\Delta_A^\perp$ ; in other words, when  $\alpha \approx \alpha_M$ , the sample is practically insensitive to the external magnetic field, and an external field amplitude as large as the irreversible field is required to reduce the critical current  $I_c$  to 67% of its zero-field value  $I_0$ .

#### IV. THEORY

In order to provide a theoretical interpretation of the experimental data presented in Sec. III, let us introduce the spatial normalized units  $\bar{x}=x/L$  and  $\bar{y}=y/W$  with the junction center coinciding with the axis origin. Our task is to find out the Josephson phase distribution  $\phi(\bar{x}, \bar{y})$  over the barrier area ( $-1 \leq \bar{x} \leq 1$  and  $-1 \leq \bar{y} \leq 1$ ) of a small planar JTJ in a weak oblique applied magnetic field  $\mathbf{H}_a$ . As a preliminary step, before resorting to Eq. (1), we need to determine the magnetic field distribution over the barrier area  $\mathbf{H}(\bar{x}, \bar{y})$ . As the Maxwell equations are linear in the magnetic field, one can resort to the principle of superposition to calculate the field  $\mathbf{H}$ . Thus, the effect of the oblique field  $\mathbf{H}_a$  can be conveniently split into the sum of the effects of two orthogonal components, that is, the in-plane component  $\sqrt{H_x^2+H_y^2}$  and the transverse one  $H_z$ . In other words,

$$\mathbf{H}(\bar{x}, \bar{y}) = \mathbf{H}^\parallel(\bar{x}, \bar{y}) + \mathbf{H}^\perp(\bar{x}, \bar{y}), \quad (7)$$

in which  $\mathbf{H}^\parallel$  and  $\mathbf{H}^\perp$  are the barrier field distributions induced by in-plane and transverse external fields, respectively.

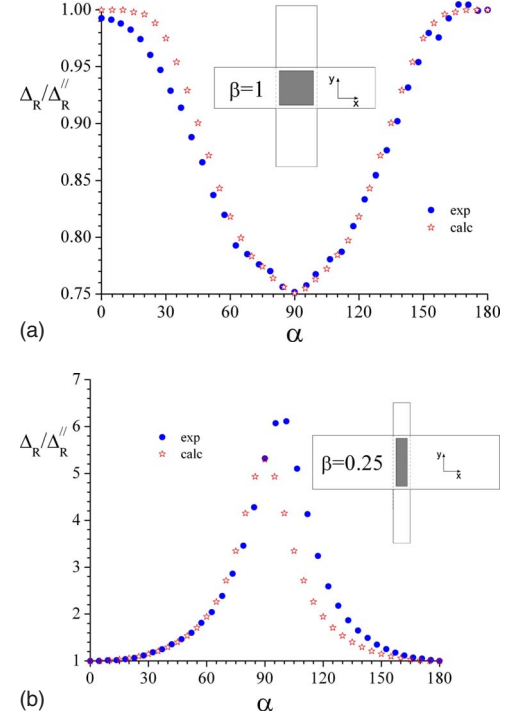


FIG. 8. (Color online) Magnetic field range  $\Delta_R$  vs  $\alpha$  (in degrees) for the two cross-type junctions of Fig. 7: (a)  $\beta=1$  and (b)  $\beta=0.25$ . The experimental data are presented by closed circles, while the open stars are the result of the calculations described in Secs. IV. The insets sketch for each sample its electrode configuration and its orientation with respect to the chosen Cartesian coordinates.

As mentioned in Sec. I, it has been traditionally assumed that when the external field lays in the barrier plane ( $H_z=0$  and  $\mathbf{H}^\perp=0$ ), it uniformly threads the oxide layer, so that  $\mathbf{H}^\parallel=\mathbf{H}=\mathbf{H}_a \equiv (H_x, H_y)$ . Today we know that this is only true to the first approximation for *naked* JTJs, since field focusing effects should be considered in planar JTJ structures especially in the case of window junctions<sup>20,21</sup> that are surrounded by a passive thick oxide layer—the so-called *idle region*.<sup>22</sup> Our samples were designed to have the smallest possible idle region, so that field focusing effects could be neglected; consequently our theory has been developed under the simplifying assumption that the samples are *naked*. Further, as shown in Fig. 1, we will only consider magnetic field directions confined to the plane specified by the angle  $\alpha$  between the applied field and the junction plane ( $H_y=0$ ). According to Eq. (7), due to the linearity of Eq. (1), also the phase distribution can be written as the sum of two terms  $\phi_\parallel(\bar{x}, \bar{y})$  and  $\phi_\perp(\bar{x}, \bar{y})$ ,

$$\phi(\bar{x}, \bar{y}) = \phi^\parallel(\bar{x}, \bar{y}) + \phi^\perp(\bar{x}, \bar{y}), \quad (8)$$

provided that  $\nabla\phi^\parallel = \kappa\mathbf{H}^\parallel \times \hat{\mathbf{z}}$  and  $\nabla\phi^\perp = \kappa\mathbf{H}^\perp \times \hat{\mathbf{z}}$ .

Once  $\phi(\bar{x}, \bar{y})$  is known, it will be possible to calculate the junction critical current  $I_c$  as<sup>14</sup>

$$I_c = I_0 \sqrt{\langle \sin \phi \rangle^2 + \langle \cos \phi \rangle^2}, \quad (9)$$

in which the brackets  $\langle \rangle$  denote spatial averages over the junction area  $4\langle f(\bar{x}, \bar{y}) \rangle = \int_{-1}^1 d\bar{x} \int_{-1}^1 d\bar{y} f(\bar{x}, \bar{y})$ .

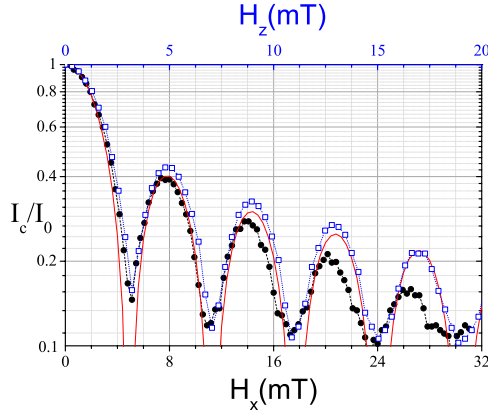


FIG. 9. (Color online) Comparison of the magnetic patterns recorded for the annular junction quoted in Table I ( $\bar{r} \approx \lambda_J$ ) in a transverse (open squares referred to top horizontal scale) and in-plane (closed circles referred to the bottom horizontal scale) applied magnetic field. The logarithmic vertical scale helps the data comparison in the lower current range. The solid line corresponds to a Bessel-type fit according to Eq. (23).

Being  $\mathbf{H}^{\parallel}=H_x\hat{x}$  (for naked small JTJs),  $\phi^{\parallel}$  is given by Eq. (2) that, with our normalization, becomes

$$\phi^{\parallel}(\bar{x}, \bar{y}) = h^{\parallel} \bar{y} \cos \alpha, \quad (10)$$

in which  $h^{\parallel}=2\pi\mu_0 H_a W d_e / \Phi_0$ , since  $H_a \cos \alpha = H_x$ . (If one wants to consider the effect of the idle region, still  $h^{\parallel} \propto H_a$ , but the proportionality constant needs proper correction.)  $\mathbf{H}^{\perp}$  and their corresponding  $\phi^{\perp}$  have been found in Ref. 9 for naked small JTJs having the most common electrode configurations. Generally speaking, it was found  $\phi^{\perp} \propto H_z = H_a \sin \alpha$ , so that we are allowed to write

$$\phi^{\perp}(\bar{x}, \bar{y}) = h^{\perp} \phi_{\perp}(\bar{x}, \bar{y}) \sin \alpha, \quad (11)$$

with  $h^{\perp} \propto H_a$  and  $\phi_{\perp}(\bar{x}, \bar{y})$  containing the spatial part of  $\phi^{\perp}(\bar{x}, \bar{y})$ . It is important to stress that the proportionality constant between  $h^{\perp}$  and  $H_a$  is not known *a priori*, being a nontrivial and still unknown function of several geometrical junction features such as the widths and the thicknesses of the two electrodes, their separation, and their configuration.<sup>9</sup> Therefore  $h^{\perp}$  remains the only free parameter when comparing the experimental data to their theoretical counterparts. Equation (8) can be now rewritten in terms of Eqs. (10) and (11) as

$$\phi(\bar{x}, \bar{y}) = h^{\parallel} \bar{y} \cos \alpha + h^{\perp} \phi_{\perp}(\bar{x}, \bar{y}) \sin \alpha.$$

Being both  $h^{\parallel}$  and  $h^{\perp}$  proportional to the intensity of the applied field  $H_a$ , their ratio  $\eta = h^{\perp}/h^{\parallel}$  depends uniquely on geometrical parameters (including the junction magnetic thickness  $d_e$ ). Therefore, the last equation can be conveniently cast in its final form,

$$\phi_{h,\alpha}(\bar{x}, \bar{y}) = h[\bar{y} \cos \alpha + \eta \phi_{\perp}(\bar{x}, \bar{y}) \sin \alpha], \quad (12)$$

in which,  $h^{\parallel}$  has simply been renamed  $h$  and the indices  $h$  and  $\alpha$  have been added to explicitly indicate that the Josephson phase distribution depends on the field strength and orientation. In the remaining part of this section, we will exten-

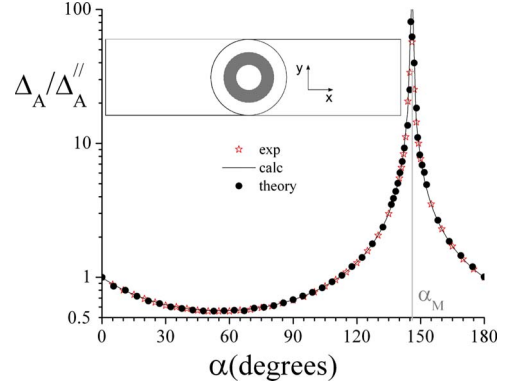


FIG. 10. (Color online) Magnetic field range  $\Delta_A$  vs  $\alpha$  (in degrees) for the annular junction quoted in Table I ( $\bar{r} \approx \lambda_J$ ). The experimental data are presented by closed circles, while the open stars are the result of calculations described in Secs. IV. The solid line arises from the approximate analytical expression (27). The inset sketches the Lyngby-type annular junction and its orientation with respect to the chosen Cartesian coordinates.

sively make use of Eq. (12), inserting—for each junction geometrical configuration—the proper  $\phi_{\perp}$  expression from Ref. 9.

### A. Overlap-type junctions

From the numerical analysis of the magnetic scalar potential induced in the barrier plane of a planar JTJ by a transverse field, we were able to derive approximate and simple expressions for the Josephson phase distribution in the barrier area that satisfy the Laplace equation ( $\partial^2 \phi / \partial x^2 + \partial^2 \phi / \partial y^2 = 0$ ). These heuristic expressions were found to be markedly dependent on the junction aspect ratio  $\beta = L/W$ . For an overlap-type junction in a unitary transverse magnetic field, we found

$$\phi_{\perp}(\bar{x}, \bar{y}) \approx \sin \bar{y} \frac{\cosh \beta \bar{x}}{\sinh \beta}, \quad (13)$$

Inserting Eq. (13) into Eq. (12), we observe that  $\phi_{h,\alpha}$  is an odd function of  $\bar{y}$ , henceforth  $\langle \sin \phi_{h,\alpha} \rangle = 0$ ; furthermore, considering that  $\phi_{h,\alpha}$  is an even function of  $\bar{x}$ , the calculation Eq. (9) of the magnetic diffraction pattern reduces to

$$I_c(h, \alpha) = I_0 \int_0^1 d\bar{x} \int_0^1 d\bar{y} \cos \phi_{h,\alpha}. \quad (14)$$

The above integral has been numerically evaluated as a function of the reduced field  $h$  and for several values of  $\alpha$ , setting  $I_0 = 3.9$  mA,  $\beta = 1$ , and  $\eta = 0.85$  in order to make a comparison with the experimental data for the square overlap junction of Figs. 4—the calculated  $I_c$  vs  $h$  are reported as dotted lines and a proper horizontal scaling was chosen to match the in-plane field range  $\Delta_R^{\parallel} = 1.29$  mT.

By construction, for  $\alpha = 0$ , Eq. (14) returns the Fraunhofer pattern. For  $\alpha \neq 0$  the calculated  $I_c(h)$ , at a quantitative level, is only consistent with the experimental data, the discrepancies being more evident for large-field values. However our calculations can grasp most of the pattern small field fea-

tures: in particular, they can nicely reproduce the dependence of the pattern width  $\Delta_R$  on  $\alpha$ , as far as  $\beta \leq 1$  [see the open stars in Figs. 5(a)–5(d)]. In fact, for  $\beta=4$ , to use expression (13) only allows us to reproduce the correct value of  $\alpha_M$ .

### B. Cross-type junctions

For a cross-type small naked JTJ with aspect ratio  $\beta$ , it was heuristically found,<sup>9</sup>

$$\phi_{\perp}(\bar{x}, \bar{y}) = \sin \bar{y} \frac{\sinh \beta \bar{x}}{\cosh \beta} + \sin \bar{x} \frac{\sinh \bar{y}/\beta}{\cosh 1/\beta}. \quad (15)$$

This approximate expression, beside satisfying the Laplace equation, has the proper symmetry properties required by the problem  $\phi_{\perp}^{\beta}(\bar{x}, \bar{y}) = \phi_{\perp}^{1/\beta}(\bar{y}, \bar{x})$ . We will consider first the relevant case of a square cross junction, i.e.,  $\beta=1$ . When this is the case, by retaining the first terms in the Taylor expansion of the trigonometric and hyperbolic functions, the above expression (15) reduces to

$$\phi_{\perp}(\bar{x}, \bar{y}) = \bar{x}\bar{y} \quad (16)$$

proposed by Miller *et al.*<sup>14</sup> in 1985. The transverse magnetic pattern of a square cross junction can be computed through Eq. (9), by inserting Eq. (15) into Eq. (8) and setting  $\alpha = \pi/2$ . The resulting  $I_c(H_z)$  is shown by the open squares in Fig. 6. Very similar results are obtained, if Eq. (15) is replaced by Eq. (16). For large fields, the calculations are well fitted by an inverse proportionality law  $I_c \propto 1/H_z$ , while the best fit to the experimental data results in a quadratically decreasing dependence  $I_c \propto H_z^{-2}$ . Again we come to the conclusion that the empirical expression taken from Ref. 9 is only valid in the small field range, in this case, as far as  $I_c(H_z) > 0.2I_0$ . Also for cross junctions, the  $I_c(H_a, \alpha)$  were calculated and the  $\alpha$  dependencies of  $\Delta_R$  were extracted and shown by the open stars in Figs. 8. In evaluating the integral (9), the parameter  $\eta$  in Eq. (12) was chosen to be equal to its experimental counterpart  $\Delta_R^{\perp}/\Delta_R^{\parallel}$ . As expected, the calculated  $\Delta_R(\alpha)$  are symmetric with respect to  $\alpha=90^\circ$ .

### C. Annular junctions

In this section, we will examine the static behavior of small annular JTJs in the presence of an oblique magnetic field. Denoting the inner and outer ring radii, respectively, as  $r_i$  and  $r_o$ , we assume that the annular junction is unidimensional, i.e., the ring mean radius  $\bar{r}=(r_i+r_o)/2$  is much larger than the ring width  $\Delta r=r_o-r_i$ .

Using polar coordinates  $r$  and  $\theta$  such that  $x=r \cos \theta$  and  $y=r \sin \theta$ , the Josephson magnetic Eq. (1) can be split into

$$\frac{\partial \phi}{\partial r} = \kappa H_{\theta}, \quad \frac{\partial \phi}{r \partial \theta} = -\kappa H_r, \quad (17)$$

where  $H_r$  and  $H_{\theta}$  are the radial and tangential components of the magnetic field in the ring plane, respectively. With the annulus unidimensional, we can neglect the radial dependence of the Josephson phase,<sup>23</sup> i.e.,  $\phi(r, \theta)=\phi(\bar{r}, \theta)$ ; henceforth,

$$\phi(\theta) = -\kappa \bar{r} \int d\theta H_r(\bar{r}, \theta) + \phi_0, \quad (18)$$

in which  $\phi_0$  is an integration constant. By resorting again to the superposition principle, we can readily write the analogous of Eqs. (7) and (8) for annular junctions as

$$H_r(\theta) = H_r^{\parallel}(\theta) + H_r^{\perp}(\theta) \quad (19)$$

and

$$\phi(\theta) = \phi^{\parallel}(\theta) + \phi^{\perp}(\theta), \quad (20)$$

provided  $\partial \phi^{\parallel} / \partial \theta = -\kappa \bar{r} H_r^{\parallel}$  and  $\partial \phi^{\perp} / \partial \theta = -\kappa \bar{r} H_r^{\perp}$ .

It is well known<sup>23</sup> that when an external field is applied in the plane of an electrically short ( $\bar{r} < \lambda_J$ ) annular junction, it fully penetrates the barrier  $\mathbf{H}^{\parallel}=H_x \hat{\mathbf{x}}$ , whose radial component  $H_r^{\parallel}=H_x \cos \theta$ , through Eq. (18), leads to

$$\phi^{\parallel}(\theta) = h^{\parallel} \sin \theta, \quad (21)$$

with  $h^{\parallel}=\kappa H_x \bar{r}$ . As far as  $\phi(\theta)$  is an odd (periodic) function, the calculation of the maximum critical current reduces to the following integration:

$$I_c = \frac{I_0}{\pi} \int_0^\pi d\theta \cos \phi(\theta). \quad (22)$$

Inserting  $\phi$  as in Eq. (21), we obtain the in-plane magnetic modulation pattern

$$I_c(h^{\parallel}) = I_0 |J_0(h^{\parallel})|, \quad (23)$$

in which  $J_0$  is the zero-order Bessel function (of first kind). In deriving Eq. (23), it was assumed that the Josephson current density is uniform over the barrier area and that no magnetic flux is trapped in between the junction electrodes [ $\phi(\theta+2\pi)=\phi(\theta)$ ]. The static properties of an annular junction in a transverse field have been numerically investigated in Ref. 9 for a Lyngby-type annular JTJ obtained by two films having the same widths;<sup>24</sup> it was found that in a first approximation,  $H_r^{\perp}$  sinusoidally depends on  $\theta$  resulting in a Bessel-type transverse magnetic pattern. In other words, small differences are expected in comparing the shapes of the in-plane and transverse magnetic diffraction patterns of an annular junction, as shown by the logarithmic graph in Fig. 9. However, a small amplitude third  $\theta$  harmonic has to be added in order to correctly reproduce  $H_r^{\perp}(\theta)$ ,

$$H_r^{\perp}(\theta) \propto H_z(\cos \theta + 3\delta \cos 3\theta), \quad (24)$$

with the coefficient  $\delta$  much smaller than unity. The last expression readily provides a more realistic  $\phi^{\perp}(\theta)$  dependence

$$\phi^{\perp}(\theta) = h^{\perp}(\sin \theta + \delta \sin 3\theta), \quad (25)$$

with  $h^{\perp} \propto H_z$ . Being  $H_x=H_a \cos \alpha$  and  $H_z=H_a \sin \alpha$ , by inserting Eqs. (21) and (25) into Eq. (20), the Josephson phase in the presence of an arbitrary oblique magnetic field applied with amplitude  $H_a=\sqrt{H_x^2+H_z^2}$  and orientation  $\alpha=\arctan(H_x/H_z)$  becomes

$$\phi_{h,\alpha}(\theta) = h[\sin \theta \cos \alpha + \eta(\sin \theta + \delta \sin 3\theta)\sin \alpha], \quad (26)$$

in which, again,  $h^\parallel$  has simply been renamed  $h$  and  $\eta = h^\perp/h^\parallel$ . In order to reproduce the experimental findings reported in Sec. III C, we have computed the  $I_c(h, \alpha)$ , inserting Eq. (26) in Eq. (22), being still  $\phi_{h,\alpha}(-\theta) = -\phi_{h,\alpha}(\theta)$ . The value of  $\eta$  has been taken from the experimental  $\Delta_A^\perp/\Delta_A^\parallel$  ratio  $\eta_A = 0.63$  from Table I, while the value of  $\delta$  was determined from the best fit of the experimental transverse magnetic pattern  $\delta = 0.02$ . The results of such calculations for several  $\alpha$  values are displayed in Fig. 10 with open stars; the agreement with the experimental data is excellent. Indeed, the third harmonic correction is mainly needed to reproduce the peak in  $\Delta_A(\alpha)$ ; in fact, with  $\delta$  set to zero, the field amplitude dependence in Eq. (26) would be undetermined for  $\alpha = -\arctan 1/\eta$ , resulting in an unphysical independence of  $I_c$  on  $H_a$ . However, far enough from this critical angle, we can set  $\delta = 0$  in Eq. (26) and the integral (22) trivially results in a Bessel-type behavior with critical field  $H_c$  or pattern width  $\Delta_A$  given by

$$\Delta_A(\alpha) = \frac{\Delta_A^\parallel}{|\cos \alpha + \eta \sin \alpha|}. \quad (27)$$

The last approximate expression plotted as a solid line in Fig. 10 exactly matches the experimental points, everywhere except near  $\alpha_M = -\arctan(1/\eta_A) \approx 145^\circ$ , where it goes to infinity. From measurements not reported in this paper, we found that Eq. (27) can be usefully applied to reproduce also the behavior of long ( $\bar{r} > 10\lambda_J$ ) unidimensional Lyngby-type annular junctions in the presence of an arbitrary oblique field.

## V. DISCUSSION

A similar approach can be adopted to describe the behavior of overlap-type junctions having the aspect ratio smaller than unity. In fact, being  $-1 \leq \bar{x} \leq 1$  and  $-1 \leq \bar{y} \leq 1$ , then  $\sin \bar{y} \approx \bar{y}$ , and, under the assumption  $\beta < 1$ ,  $\cosh \beta \bar{x} \approx 1$ . Therefore, Eq. (12) simplifies to a linear  $\bar{y}$  dependence

$$\phi(\bar{x}, \bar{y}) = h(\cos \alpha + \eta \sin \alpha) \bar{y},$$

resulting in a Fraunhofer-type magnetic diffraction pattern with  $H_c$  or, with our notation  $\Delta_R$ , given by

$$\Delta_R(\alpha) = \frac{\Delta_R^\parallel}{|\cos \alpha + \eta \sin \alpha|} = 1/\left|\frac{\cos \alpha}{\Delta_R^\parallel} + \frac{\sin \alpha}{\Delta_R^\perp}\right|. \quad (28)$$

It's seen that the critical width  $\Delta_R$  diverges at a critical angle  $\alpha_c$  given by

$$\alpha_c = -\arctan \frac{1}{\eta} = -\arctan \frac{\Delta_R^\parallel}{\Delta_R^\perp}. \quad (29)$$

In other words, when  $\alpha = \alpha_c$ , the effect of the transverse component of the applied magnetic field exactly cancels that of the in-plane component, so that the junction is virtually insensitive to the magnetic field. In practice, a full compensation is never achieved, although  $\Delta_R(\alpha_M)$  can be as large as

$100\Delta_R^\parallel$ . Equation (28) is plotted as a solid line in Figs. 5(a)–5(c) and it is seen that it nicely reproduces the experimental data not only when  $\beta < 1$  [see Fig. 5(b)] but also for  $\beta = 1$  [see Fig. 5(a)]. It also closely fits the results of a long ( $2W = 12\lambda_J$ ) unidimensional JTJ [see Fig. 5(c)] for which the calculations developed in Sec. IV A for electrically small junctions do not apply. Equations (27) and (28) indicate that for small unidimensional annular junctions and small overlap-type junctions with small aspect ratio, only two measurements are needed to forecast their static behavior in an arbitrary oblique field, that is, the in-plane and the transverse magnetic diffraction patterns.

As far as cross-type samples JJ#E and JJ#F are concerned, we observe that the experimental data shown, respectively, in Figs. 5(a) and 5(b) are affected by a slight asymmetry with respect to  $\alpha = 90^\circ$ , in contrast with the system symmetry properties (even in the case of electrically long junctions). We explain this symmetry break in terms of tiny fabrication misalignments. In our fabrication line, once the base electrode has been etched away, each next layer is positioned with an accuracy better than  $1 \mu\text{m}$  (in each direction). This accuracy, although smaller, is comparable with the idle-region dimension, resulting in an unavoidable—albeit small—imperfection in positioning the junction area exactly in the centers of the films. Since the screening currents mainly flow along the electrode borders, the misalignment effect increases with the junction side dimension. This explains why the observed asymmetry is larger for junction #F.

For the Lyngby-type annular junction, our theory reproduces the experimental data in a more than satisfactory fashion. However, the situation might be not so good for annular junctions made by electrodes of unequal widths as, for example, those used in Ref. 18, which require also the introduction of the second  $\theta$  harmonic in Eq. (24). However, when  $\phi^\perp(\theta)$  is as in Eq. (25), exploiting the trigonometric equivalence  $\sin 3x = \sin x(1+2 \cos 2x)$ , the transverse magnetic pattern can be analytically shown to be given by the following even expression:

$$I_c(h^\parallel) = I_0 |J_0(h^\parallel) + 2\delta J_2(h^\parallel)|,$$

in which  $J_2$  is the second-order Bessel function and  $\delta$  was assumed to be much smaller than unity. Similarly,  $I_c(h)$  can be analytically worked out in the more general case of Eq. (26), as far as  $\alpha$  is far from  $\alpha_M$ , more precisely, when  $\delta \ll 1 + 1/\eta_A \tan \alpha$ .

The weak point of our theoretical approach based on the superposition principle is the indetermination of the parameter  $h^\perp$  introduced in Eq. (11). The knowledge of the magnetic field actually introduced into the barrier for a given transverse field  $H_z$  requires a careful experimental investigation with samples having a given junction geometry and different geometrical parameter of the connecting electrodes. However, while the superconducting film widths can be easily varied, it is difficult to realize samples with much different film thicknesses. Consequentially, when the shape of the  $I_c(H_z)$  is known *a priori*, the effective normalized field  $h^\perp$  remains to be determined from the direct measure of the transverse magnetic diffraction pattern.

## VI. CONCLUSION

In this paper, we examined the static properties of small planar Josephson tunnel junction in presence of a uniform external field applied at an arbitrary angle with respect to the barrier plane. This topic has been considered from both the experimental and theoretical point of view. We have presented the recorded oblique magnetic diffraction patterns of junctions with the most common electrode configuration, namely, overlap, cross, and annular geometries. These data, beside being original by themselves, also served as a test for the theoretical analysis of small JTJs in a purely transverse field that we recently proposed.<sup>9</sup> Further, by invoking the superposition principle, the findings of Ref. 9 in a transverse field were combined with the classical knowledge for a JTJ in a parallel field to provide a general theory for any arbitrary oblique field. We stress that the theory has been developed assuming that junction was electrically small, naked, geometrically perfect, and made with purely diamagnetic superconducting films ( $\lambda_L=0$  and  $H_c=\infty$ ). Although our samples satisfied these conditions only to a rough approximation, the agreement between the experimental and theoretical results is more than satisfactory especially for annular junctions. For rectangular samples, the theoretical approach is again very good only for small values of the applied field and of the junction aspect ratio. In the other cases, our theoretical predictions fail to provide a correct description. This was to be expected because the approximate analytical expressions heuristically found in Ref. 9 were already observed to have the largest relative error near the junction corners. As already reported elsewhere,<sup>14</sup> the importance of the Josephson phase at the junction corners grows with the amplitude of the external field.

The main message of this paper is that even a small transverse field (which has been largely ignored in the past) can strongly influence the magnetic interference patterns. We explore the implications of this result in supposing systematic errors in previous experiments and in proposing different possible applications. Since in most of the applications the external field needed to modulate the critical current of a planar JTJ is applied in the barrier plane by means of a long solenoid or Helmholtz coil pairs, we want to stress the importance of the alignment of the solenoid (or coil) axis with the junction plane. It was believed that any possible tiny angular misalignment  $\delta\alpha$  between the coil axis and the junction plane would result in only second-order errors, being  $H_x=(1-0.5\delta\alpha^2)H_a$ . However, as we have shown, this is not necessarily true, since the unwanted (and often unknown) small transverse field component  $H_z=\delta\alpha H_a$  might have an effect comparable or even larger than that of the in-plane

component, if the junction critical angle  $\alpha_c$  is close to  $180^\circ$ . For example, in the case of sample JJ#C of Table I, a misalignment  $\delta\alpha=-4^\circ$  would result in a systematic error of more than 1 order of magnitude for the measurement of the first critical field. The consequence of the coil misalignment might have been underestimated, if not ignored, in many previous experiments dealing with JTJs in an external magnetic field, including those in which the exact knowledge of the field in the barrier plane is of capital importance. As a corollary, it also follows that in shielding a cryoprobe the same care has to be taken to minimize both the in-plane and the transverse stray fields.

Furthermore, in planar superconducting quantum interference device (SQUID) applications, the magnetic field to be measured is applied perpendicular to the SQUID loop and its effect on the junction critical currents has never been considered. However, it might not be negligible, especially when the field is large and the junction(s) is placed close to the borders of the superconducting electrodes where the induced screening currents are larger—this is the case of step-edge or ramp-type junctions.<sup>25,26</sup>

In this paper, we have shown that for a given junction geometry the response to an externally applied magnetic field drastically depends on the field orientation; a property that might be exploited to design angle resolving instruments. Furthermore, considering that this response is different for JTJs having different geometries, it makes possible to design multijunction chips in which, for a given applied magnetic field, the critical current of some junctions is almost completely suppressed while that of other junctions remains unaffected. Our findings also suggest that two (or more) independent magnetic fields with different amplitudes and orientations can be applied to multijunction chips in order to obtain the proper critical current suppression required for samples having different geometrical configurations.

By using Eq. (4), the theory developed in Sec. IV for a uniform oblique field applied in the  $y=0$  plane can be easily extended to the most general case in which all three field components are nonzero. In other words, the oblique magnetic diffraction pattern can be theoretically predicted for the most common junction configurations, as far as the junction dimensions are smaller than Josephson penetration length. The case of long JTJ in a transverse field still remains an open question since it requires the solution of a tridimensional magnetostatic problem in the presence of external (nonlinear) currents.

## ACKNOWLEDGMENT

We thank Pavel Dmitriev for the fabrication of the samples.

\*roberto@sa.infn.it

<sup>1</sup>J. M. Rowell, Phys. Rev. Lett. **11**, 200 (1963); M. D. Fiske, Rev. Mod. Phys. **36**, 221 (1964).

<sup>2</sup>R. F. Broom, J. Appl. Phys. **47**, 5432 (1976).

<sup>3</sup>B. D. Josephson, Rev. Mod. Phys. **36**, 216 (1964).

<sup>4</sup>A. Barone and G. Paternò, *Physics and Applications of the Josephson Effect* (John Wiley & Sons, New York, 1982).

<sup>5</sup>A. F. Hebard and T. A. Fulton, Phys. Rev. Lett. **35**, 1310 (1975).

- <sup>6</sup>I. Rosenstein and J. T. Chen, Phys. Rev. Lett. **35**, 303 (1975).
- <sup>7</sup>L. D. Landau and E. M. Lifshitz, *Electrodynamics of Continuous Media* (Addison-Wesley, Reading, 1960).
- <sup>8</sup>E. H. Brandt, Phys. Rev. B **72**, 024529 (2005), and references therein.
- <sup>9</sup>R. Monaco, M. Aaroe, J. Mygind, and V. P. Koshelets, J. Appl. Phys. **104**, 023906 (2008).
- <sup>10</sup>V. P. Koshelets, S. V. Shitov, A. V. Shchukin, L. V. Filippenko, I. L. Lapitskaya, and J. Mygind, “*Integrated Flux-Flow Oscillators for Sub-MM Wave Receivers*,” Proceedings of the International Conference on Nonlinear Superconducting Devices and HTc Materials, Capri, Italy, (1994), edited by R. D. Parmentier and N. F. Pedersen (World Scientific, Amsterdam, 1995), pp. 383–401; Valery P. Koshelets, Sergey V. Shitov, Alexey V. Shchukin, and Lyudmila V. Filippenko, Appl. Phys. Lett. **69**, 699 (1996).
- <sup>11</sup>R. Cristiano, L. Frunzio, R. Monaco, C. Nappi, and S. Pagano, Phys. Rev. B **49**, 429 (1994).
- <sup>12</sup>M. Weihnacht, Phys. Status Solidi **32**, K169 (1969).
- <sup>13</sup>R. L. Peterson, Cryogenics **31**, 132 (1991).
- <sup>14</sup>S. L. Miller, K. R. Biagi, J. R. Clem, and D. K. Finnemore, Phys. Rev. B **31**, 2684 (1985).
- <sup>15</sup>N. Martucciello and R. Monaco, Phys. Rev. B **54**, 9050 (1996).
- <sup>16</sup>M. Breitwisch and D. K. Finnemore, Phys. Rev. B **62**, 671 (2000), and references therein.
- <sup>17</sup>R. Monaco, M. Aaroe, J. Mygind, and V. P. Koshelets, J. Appl. Phys. **102**, 093911 (2007).
- <sup>18</sup>R. Monaco, J. Mygind, M. Aaroe, R. J. Rivers, and V. P. Koshelets, Phys. Rev. Lett. **96**, 180604 (2006).
- <sup>19</sup>M. Aaroe, R. Monaco, V. P. Koshelets, and J. Mygind (unpublished).
- <sup>20</sup>R. Monaco, G. Costabile, and N. Martucciello, J. Appl. Phys. **77**, 2073 (1995).
- <sup>21</sup>A. Franz, A. Wallraff, and A. V. Ustinov, J. Appl. Phys. **89**, 471 (2001).
- <sup>22</sup>J. G. Caputo, N. Flytzanis, and M. Devoret, Phys. Rev. B **50**, 6471 (1994).
- <sup>23</sup>N. Martucciello and R. Monaco, Phys. Rev. B **53**, 3471 (1996).
- <sup>24</sup>A. Davidson, B. Dueholm, B. Kryger, and N. F. Pedersen, Phys. Rev. Lett. **55**, 2059 (1985).
- <sup>25</sup>M. Podt, J. Flokstra, and H. Rogalla, Supercond. Sci. Technol. **16**, 1394 (2003).
- <sup>26</sup>H. J. H. Smilde, Ariando, D. H. A. Blank, H. Hilgenkamp, and H. Rogalla, Phys. Rev. B **70**, 024519 (2004).